Journal of ELECTRONIC MATERIALS, Vol. 48, No. 5, 2019
https://doi.org/10.1007/s11664-019-06941-0
© 2019 The Author(s)

Influence of Zn Concentration on Interfacial Intermetallics During Liquid and Solid State Reaction of Hypo and Hypereutectic Sn-Zn Solder Alloys

H.R. KOTADIA,[1,2,4] S.H. MANNAN,[2] and A. DAS[3]

1.—Warwick Manufacturing Group, The University of Warwick, Coventry CV4 7AL, UK. 2.—Department of Physics, King's College London, Strand, London WC2R 2LS, UK. 3.—Materials Research Centre, College of Engineering, Swansea University Bay Campus, Fabian Way, Swansea SA1 8EN, UK. 4.—e-mail: H.Kotadia@warwick.ac.uk

In this study, Sn-Zn solder samples containing 2 to 12 wt.% Zn were fabricated and reflowed into a Cu substrate. The microstructure of solder samples was observed after reflow and aging for up to 1000 h at 150°C. Thermodynamically stable intermetallics (IMCs) Cu-Zn and Cu-Sn formed at the interface depending on the solder composition. Formation of different interfacial IMCs during soldering and after prolonged aging is explained by the spalling mechanism that resulted from the depletion of Zn from the solder matrix.

Key words: Soldering, intermetallics, wettability, spalling, lead-free solder, Sn-Zn alloys

INTRODUCTION

The last two decades have seen accelerated global research efforts into developing Pb-free Sn-based solders for the electronics industry. Three solder systems, Sn-Cu, Sn-Ag, and Sn-Ag-Cu, have emerged as the front runners to replace the low temperature Sn-Pb solders despite limited reliability.[1] The eutectic Sn-Cu solder (Sn-0.7Cu, wt.%) is considered a promising candidate for the wave soldering, and it also presents financial cost advantages compared to Ag containing alternatives.[2] However, many problems have been reported for all three solders, such as excessive growth of Cu_6Sn_5 (η phase) and Cu_3Sn (ε phase) IMC and Kirkendall void forming at the Cu_3Sn/Cu interface due to the deficient Sn flux during the phase transformation during the high temperature storage.

Some studies have also been conducted on Sn-9Zn (melting point 198°C) eutectic solder, which could offer better mechanical properties, as a possible replacement for Sn–Pb solder (melting temperature 183°C).[1,3,4] Zn has a high tendency of oxidation and corrosion, which restricts its application in the packaging industry. An improvement in wettability, resulting from the reduction in surface tension of Sn-Zn solder alloys, is observed through the addition of Bi, Ag, Al, RE (In, Ce, La, Nd) and active flux under a N_2 atmosphere.[4–6] Also, trace addition of Bi, In and Ga can reduce the melting temperature of Sn-Zn eutectic alloy significantly.[4,7] The effect of Zn as a minor element was studied by Kotadia et al.[8–11] and others[12–14] in the Sn-Cu, Sn-Ag, and Sn-Ag-Cu solder systems. These studies concluded that Cu-Zn and Cu-Sn interfacial IMCs form during soldering at ~ 1.5 wt.%Zn/Cu liquid reaction and that the Cu-Zn layer acts as a barrier layer even under higher temperature aging. For Zn concentration less than 1.5 wt.% in the base solder, Zn diffuses into the Cu_6Sn_5 IMCs, effectively suppressing interfacial IMC growth and Kirkendall voids by suppressing Cu_3Sn IMC formation during aging, which subsequently improves the shear strength of the solder joint.[11]

In addition to that, solder joints are constantly subjected to a wide range of temperature (−40°C to 150°C or even higher), especially in automotive, aerospace and traction applications. This thermal

(Received October 9, 2018; accepted January 8, 2019; published online January 23, 2019)

cycling makes a solder joint ($Cu_6Sn_5/Cu_3Sn/Cu$) weak from 2.15% volume expansion/contraction through the $\eta \rightarrow \eta' - Cu_6Sn_5$ polymorphic phase transformation that may lead to cracking in severe cases.[15] Previous experimental studies have shown that addition of Zn can stabilise hexagonal $\eta - Cu_6Sn_5$ crystal structure.[16,17]

Following our previous work,[8–11] a comparative study of the hypo and hyper-eutectic Sn-Zn solder alloys have been undertaken after reflow and high temperature storage at 150°C for 1000 h to gain a better understanding of the effect of Zn on the interfacial reaction with Cu substrate, on the microstructure of the solder joint and on the solidification process.

EXPERIMENTAL PROCEDURES

The alloys were prepared by melting 99.9% purity Sn and Zn ingots in an alumina crucible using an electric resistance furnace operating at 420°C. After homogenising the melt for 20 min, cylindrical samples were cast. Zn vaporisation and oxidation was minimised during alloy preparation by selecting low smelting temperature and holding time. Melting and solidification of all the prepared alloys were also investigated using a Mettler Toledo DSC 822 differential scanning calorimeter. For each alloy composition, approximately 20 mg samples were investigated under heating/cooling rates of 1, 5, and 10°C/min between 25°C and 250°C. The measurements were performed twice for each condition to ensure reproducibility. Soldering experiments were carried out on approximately 5 mm square plates consisting of ~ 35 μm Cu coated FR4 substrate. The substrate was cleaned using IPA (isopropyl alcohol), acetone and, finally, deionised water. For all the alloys, a 0.010 ± 0.003 g solder sample was cut from the solidified ingot, cleaned, coated by a thin layer of Henkel LF318 flux, and placed with approximately 1 mm layer thickness onto the substrate. Reflow was carried out by preheating at 140°C for 150 s in air and soldering at 260°C for 60 s. High temperature storage of the solder alloy samples was investigated at 150°C for 1000 h in air to reveal the modification in IMC growth kinetics under solid-state reactions. The samples were polished using standard metallographic techniques and examined using a ZEISS AxioLab A1 optical microscope and an FEI Quanta FEG SEM equipped with energy-dispersive x-ray spectroscopy (EDX) to identify the microstructure and the compositions of observed phases.

RESULTS

Figure 1a shows typical DSC traces for all solder systems during both the heating and cooling experiments. Upon heating, the major exothermic peak observed at lower temperature indicates melting of the eutectic phase while a minor peak observed at higher temperature indicates melting of the primary (terminal) solid. On cooling, corresponding endothermic peaks were observed with a high temperature minor peak belonging to the terminal phase (when present) and the low temperature principle peak belonging to the freezing of the Sn-Zn eutectic. Micrographs from the DSC samples are presented in Fig. 1b for correlation with the DSC results. The general features of the DSC profiles and associated micrographs agree well with the binary Sn-Zn phase diagram. For the Sn-2Zn and Sn-5Zn alloys, the minor DSC peak (besides the eutectic) belongs to solidification of the primary Sn phase that are observed to solidify dendritically (light phase in Fig. 1b and c). Sn-9Zn being closest to the eutectic composition (Sn-8.8Zn), there is a minimal amount of primary Zn solidification (dark plates in Fig. 1d). The amount of primary Zn solidification in the Sn-12Zn alloy is more noticeable in the micrograph (Fig. 1e) with longer dark Zn-plates of 1–2 mm length. However, the overall quantity of primary Zn solidified is minor resulting in no noticeable primary solidification/melting peak being observed in the DSC trace for the Sn-12Zn alloy.

Figure 2a–d shows the solder wetting angle of the Sn-Zn/Cu joints after soldering at 260°C. The wettability of the solder alloy changes with the amount of Zn addition into the Sn. The addition of Zn is observed to progressively increase the measured contact angle from 55.4° (Sn-2Zn) to 69.8° (Sn-12Zn). This increase has been attributed to the oxidation of Zn atoms at the molten solder surface. The literature suggest that overheating causes reduction in the wetting angle until 6.5 wt.%Zn addition into Sn, while further addition significantly increase wetting angle due to the higher Zn oxidation.[18] However, the current experimental results do not follow a similar trend, which might be due to the difference in experimental procedure.

Figure 2e–h also shows the cross-sectional SEM micrographs of the Sn-Zn/Cu interface after aging at 150°C for 1000 h. As shown in Fig. 2, the microstructure of the solder after reflow consists of β-Sn matrix (white phase) and fine rod-shaped Zn flakes (dark phase), similar to the microstructure of the solder alloys shown in Fig. 1. It is clearly evident from Fig. 2a to d that the eutectic volume fraction increases with Zn concentration, and in the hypereutectic 12 wt.% Zn alloy some primary Zn flakes grow from the interfacial IMC. These long Zn rich flakes are believed to have a detrimental effect on solder joint reliability by nucleating and propagating cracks. Also, crack nucleation is more severe when the solder joint is under thermal cycling and impact loading. Similar behaviour has been reported for Ag_3Sn IMC in Sn-Ag-Cu solder/Cu joints by previous researchers.[19] Figure 2 shows that a scallop shaped interfacial IMC layer formed at the solder/copper interface at low Zn concentration, but that as Zn concentration increases, this layer becomes more prominent after reflow.

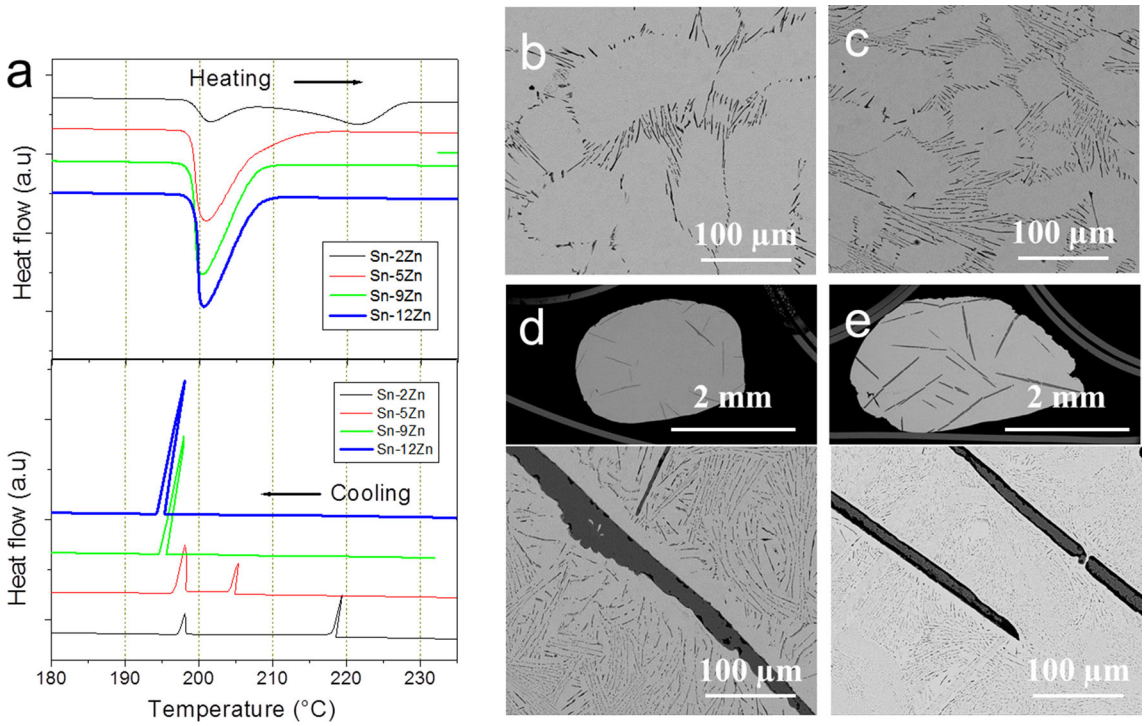

Fig. 1. (a) DSC traces at 5°C/min heating/cooling rate for Sn-XZn (X = 2, 5, 9 and 12 wt.%Zn) solders. SEM micrographs from the DSC samples are presented for (b) Sn-2Zn, (c) Sn-5Zn, (d) Sn-9Zn and (e) Sn-12Zn solders. White and black phases represent β-Sn and Zn-rich phases, respectively.

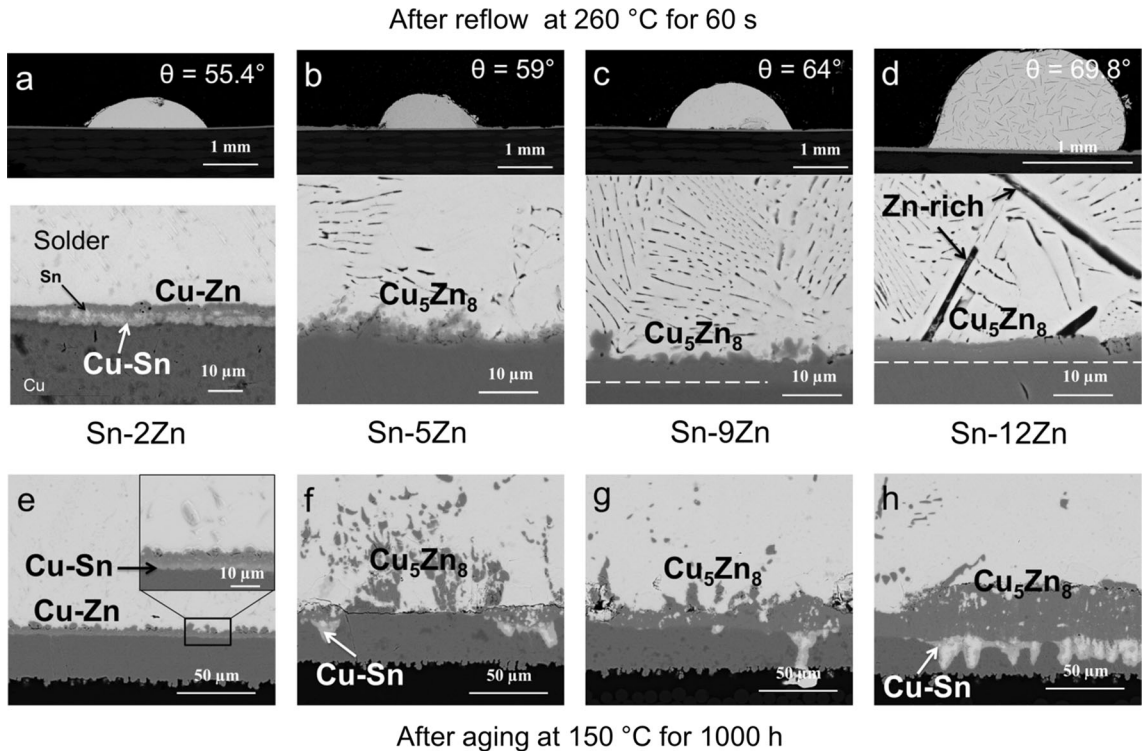

Fig. 2. SEM micrographs from the Sn-XZn/Cu systems (a)–(d) after reflow at 260°C and (e)–(h) after aging at 150°C for 1000 h. Figs. (a)–(d) shows solder wetting angle and complete solder joint morphology and in (e) inset shows Cu-Zn and Cu-Sn interfaical IMCs at high magnification. The dashed white line in figure (c) and (d) is drawn to separate Cu_5Zn_8 interfacial IMC and Cu substrate. All phases are denoted by their binary formulae.

Figure 2a shows that two different interfacial IMC form; one is Cu-Zn with 47.37 at.% Zn, and the other is Cu_6Sn_5 (< 1 μm thickness) with 5.77 at.% Zn concentration. The Cu-Zn layer is seen as porous with 12.86 wt.% Sn, however, due to the similar concentration of Cu and Zn, only CuZn IMC is considered in the manuscript. All phases are denoted in their binary formulae. In Fig. 2b, IMC at the Sn-5Zn solder/Cu substrate interface is very thin (average thickness 2.06 μm) in comparison with other systems and was confirmed to be Cu_5Zn_8 by EDX analysis. For Cu-9Zn and Cu-12Zn/Cu systems, stable Cu_5Zn_8 IMC of approximately $\sim$ 4 μm thickness formed.

In general, interfacial IMCs grew with increasing aging time and temperature due to increased solid-state diffusion of Cu atoms from the substrate and Sn and/or Zn atoms from the solder matrix. At 150°C, Cu is the dominant diffusion species as indicated by the reduction in the thickness of Cu substrate. Also, Sn and/or Zn atoms diffuse by the vacancy-diffusion mechanism and react with the Cu substrate. The nature of the IMCs, however, depends on the interfacial IMC stability and on the specific conditions. Figure 2e to h shows alteration of interfacial IMCs after aging at 150°C for 1000 h compared with that after reflow (Fig. 2a to d). For the Sn-2Zn solder system (Fig. 2e), it is evident that the Cu-Zn based barrier layer remained unchanged even after 1000 h aging and acts as a barrier suppressing Cu_6Sn_5 and Cu_3Sn IMCs formation, consistent with prior observations on other Sn-based solders with Zn addition.[8,9] In contrast, for Sn-5 to 12 wt.%Zn solder joints, the layer-type Cu_5Zn_8 IMC was discontinuous due to the spalling after 1000 h ageing, which opens up channels for the Sn from the solder to react with the Cu from the substrate, eventually forming Cu-Sn based IMCs at the interface (Fig. 2f–h). Table I summarises all observed interfacial IMC compositions.

Table I. Composition (at.%) of the interfacial intermetallics after 1000 h aging at 150°C. Each composition is calculated from the average of six EDS spectra obtained from the intermetallics along the joint

Sample	Sn	Cu	Zn
Sn-2Zn/Cu	–	51.99	48.01
	52.29	43.31	4.4
Sn-5Zn/Cu	–	43.41	56.59
	43.48	56.52	–
Sn-9Zn/Cu	–	37.90	62.10
	35.86	64.14	–
Sn-12Zn/Cu	–	36.44	63.56
	38.59	61.41	–

DISCUSSION

In all the four solders, the reactive element Zn actively participates in the formation of interfacial IMC and eutectic phase. Isothermal section of the Sn-Zn-Cu ternary system at 250°C, which is very close to the soldering temperature (260°C),[20] is used here to explain the IMC formation and evolution at the substrate interface. The liquid (Sn) phase has tie-lines with the $CuZn_5$, Cu_5Zn_8, CuZn and Cu_6Sn_5 phases, respectively, with decreasing Zn concentration in the (Sn) alloy. The reaction product changes from single phase Cu_6Sn_5 (Sn/Cu) to two phases Cu_6Sn_5 + CuZn (Sn-2Zn/Cu) and then to single-phase Cu_5Zn_8 (Sn-(5-12)Zn/Cu) as the initial Zn concentration increases for the reflowed sample (Fig. 2). Thickness of the Cu_5Zn_8 IMC also increased with the Zn concentration in the Sn solder (Fig. 3).

The phenomenon of IMC spalling has been seen in several solder systems,[21–24] including previous studies of Zn containing solders.[8–10] This is caused by the depletion of Zn as it is consumed in the production of the original IMC. As the solder is depleted of this active element, the original interfacial IMC no longer remains the thermodynamically stable IMC at the solder/substrate interface, resulting in spalling of the original layer. With 2 wt.% Zn, two IMC layers (CuZn and Cu_6Sn_5) formed at the Sn-2Zn/Cu solder-substrate interface (Fig. 2a). As seen in Fig. 2a, during soldering nearly all Zn is consumed to form a CuZn layer that will

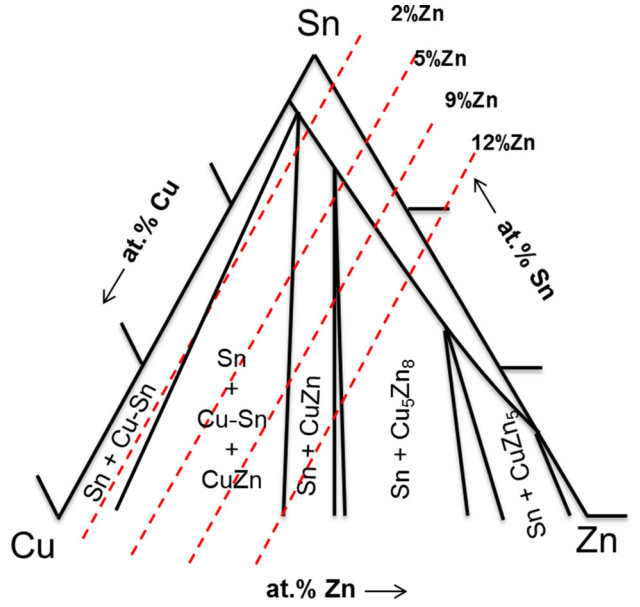

Fig. 3. Isothermal section of the Sn-Zn-Cu ternary system at 250°C (data was used from Ref. 20). Dashed red lines are used to trace the microstructural evolution and phase formation in the investigated Sn-Zn solder alloys with progressive increase in Cu concentration. This is representative of the microstructure evolution at the solder-substrate interface.

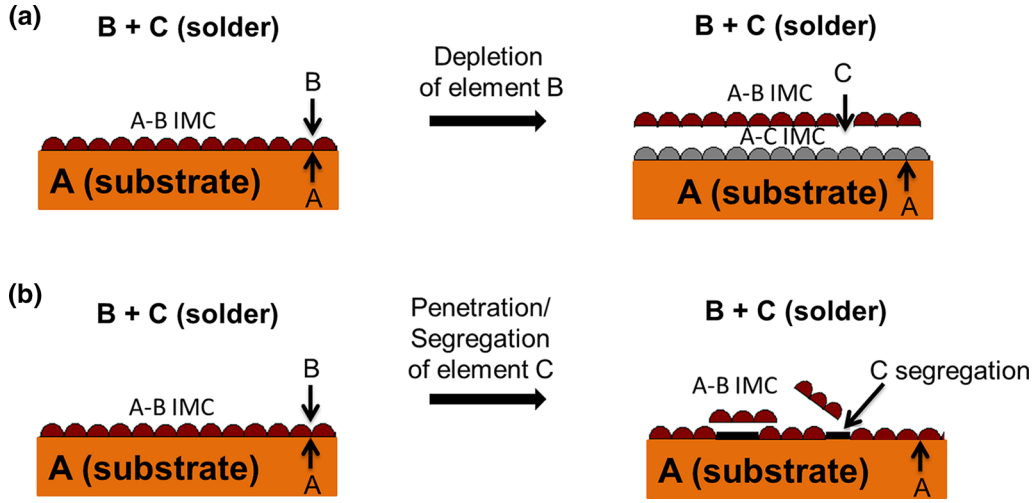

Fig. 4. Schematic illustration of different spalling mechanisms (a) due to the depletion of alloying elements either from the solder or the substrate; (b) due to the penetration and segregation and/or interruption of interfacial reaction.

lead to lesser Zn rich eutectic formation and subsequent alteration of the solidification path (Fig. 1b).

It appears that 2 wt.% Zn addition to pure Sn can suppress interfacial IMC even after 1000 h aging. Moreover, no voids form within the IMC layer or its interfaces and minor Zn addition can stabilize the Cu_6Sn_5 hexagonal structure during the thermal aging process, which effectively improves solder joint reliability.[15–17]

Addition of 5–12 wt.% Zn shows a single layer of Cu_5Zn_8 interfacial IMC formation during soldering, as predicted from the ternary phase diagram. During the aging process, the remaining Zn in the solder bulk is progressively consumed with increasing aging time. As a result, the interface between Cu and Cu_5Zn_8 becomes unstable, as Cu-Sn IMCs become the stable interfacial IMC. Change is observed in the interfacial structure with the IMC spalling off and allowing the new thermodynamically stable Cu_6Sn_5 and Cu_3Sn IMC to grow at the interface during the aging process. For Sn-5Zn the rate of spalling of Cu_5Zn_8 is high as the change in stable interfacial IMC occurs quickly as Zn is depleted. Hence, a distinct interface is observed which could lead to the crack initiation and propagation as evidenced in Fig. 2f. For Sn-(9-12) wt.% Zn/Cu systems, the amount of Zn in the solder matrix is higher than that for the Sn-5Zn solder so that the change in stable interfacial IMC occurs more gradually. As a result, the Cu_5Zn_8 IMC spalling rate is lower and no crack is observed after 1000 h of aging. However, if these solder samples are continuously aged for longer time, then they are predicted to perform very similarly to the Sn-5Zn solder system.

From the current work and existing literature[8–10,21–24] two primary origins of spalling occurring in the solder system can be suggested: (1) depletion of elements actively involved in interfacial IMC formation; this depletion is largely determined by the solder composition, solder volume, soldering and aging time; (2) penetration and segregation of elements at the interface with reaction time, which interrupts the interfacial IMC reaction and leads to loss of chemical adhesion at the interface. Figure 4 shows a schematic diagram illustrating the different spalling phenomena. In many cases, spalling occurs where both mechanisms work together to create new thermodynamically stable interfacial IMC that is in equilibrium with the solder.

CONCLUSIONS

From the present investigation, the following conclusions can be drawn:

1. Thermodynamically stable Cu_6Sn_5, Cu_3Sn, CuZn and Cu_5Zn_8 interfacial IMCs form after reflow and aging subject to the solder composition and treatment conditions.
2. The solder contact angle at the substrate is increased from 55.4° to 69.8° by increasing Zn from 2 to 12 wt.% into pure Sn. Zn oxidation played a dominate role on wetting even though reflow was carried out in the presence of flux.
3. In the Sn-2Zn/Cu system, CuZn IMC formed as a stable barrier at the interface during soldering while in the Sn-(5-12)Zn/Cu system, Cu_5Zn_8 spalled away from the interface during the aging allowing the formation of stable Cu-Sn IMC at the interface. Spalling occurs due to the depletion of Zn from the solder matrix.

ACKNOWLEDGMENTS

This research was funded by the Engineering and Physical Sciences Research Council (Grant No. EP/G054339/1) in collaboration with Henkel Technologies, Dynex, and Schlumberger.

OPEN ACCESS

This article is distributed under the terms of the Creative Commons Attribution 4.0 International License (http://creativecommons.org/licenses/by/4.0/), which permits unrestricted use, distribution, and reproduction in any medium, provided you give appropriate credit to the original author(s) and the source, provide a link to the Creative Commons license, and indicate if changes were made.

REFERENCES

1. H.R. Kotadia, P.D. Howes, and S.H. Mannan, *Microelectron. Reliab.* 54, 1253 (2014).
2. E. Bradley, C.A. Handwerker, J. Bath, R.D. Parker, and R.W. Gedney, *Lead-Free Electronics: iNEMI Projects Lead to Successful Manufacturing* (New York: Wiley, 2007).
3. R.A. Islam, B.Y. Wu, M.O. Alam, Y.C. Chan, and W. Jillek, *J Alloys Compd.* 392, 149 (2005).
4. M. McCormack, S. Jin, H. Chen, and D. Machusak, *J. Electron. Mater.* 23, 687 (1994).
5. H. Wang, S. Xue, W. Chen, and F. Zhao, *J. Mater. Sci. Mater. Eletron.* 20, 1239 (2009).
6. L. Zhang, S.-B. Xue, L.-L. Gao, Z. Sheng, H. Ye, Z.-X. Xiao, G. Zeng, Y. Chen, and S.-L. Yu, *J. Mater. Sci. Mater. Eletron.* 21, 1 (2010).
7. R.K. Shiue, L.W. Tsay, C.L. Lin, and J.L. Ou, *Microelectron. Reliab.* 43, 453 (2003).
8. H.R. Kotadia, O. Mokhtari, M. Bottrill, M.P. Clode, M.A. Green, and S.H. Mannan, *J. Electron. Mater.* 39, 2720 (2010).
9. H.R. Kotadia, O. Mokhtari, M.P. Clode, M.A. Green, and S.H. Mannan, *J Alloys Compd.* 511, 176 (2012).
10. H.R. Kotadia, A. Panneerselvam, O. Mokhtari, M.A. Green, and S.H. Mannan, *J. Appl. Phys.* 11, 074902 (2012).
11. H.R. Kotadia, A. Panneerselvam, M.W. Sugden, H. Steen, M. Green, S.H. Mannan, and I.E.E.E. Trans, *Compon. Packag. Manuf. Technol.* 3, 1786 (2013).
12. F. Wang, X. Ma, and Y. Qian, *Scrip. Mater.* 53, 699 (2005).
13. Y.K. Jee, Y.H. Ko, and J. Yu, *J. Mater. Res.* 22, 1879 (2011).
14. S.K. Kang, D.-Y. Shih, D. Leonard, D.W. Henderson, T. Gosselin, S.-I. Cho, J. Yu, and W.K. Choi, *JOM* 56, 34 (2004).
15. F. Somidin, H. Maeno, M.A.A. Mohd Salleh, X.Q. Tran, S.D. McDonald, S. Matsumura, and K. Nogita, *Mater. Char.* 138, 113 (2018).
16. G. Zeng, S.D. McDonald, Q. Gu, and K. Nogita, *J. Mater. Res.* 27, 2609 (2012).
17. C.-Y. Yu and J.-G. Duh, *Scrip. Mater.* 65, 783 (2011).
18. X. Wei, H. Huang, L. Zhou, M. Zhang, and X. Liu, *Mater. Lett.* 61, 655 (2007).
19. K.S. Kim, S.H. Huh, and K. Suganuma, *J Alloys Compd.* 352, 226 (2003).
20. C.Y. Chou and S.W. Chen, *Acta Mater.* 54, 2393 (2006).
21. M.D. Cheng, S.Y. Chang, S.F. Yen, and T.H. Chuang, *J. Electron. Mater.* 33, 171 (2004).
22. J.-W. Jang, L.N. Ramanathan, J.-K. Lin, and D.R. Frear, *J. Appl. Phys.* 95, 8286 (2004).
23. J.W.R. Teo and Y.F. Sun, *Acta Mater.* 56, 242 (2008).
24. K.-Z. Wang and C.-M. Chen, *J. Electron. Mater.* 34, 1543 (2005).